

RSC Advances



This is an *Accepted Manuscript*, which has been through the Royal Society of Chemistry peer review process and has been accepted for publication.

Accepted Manuscripts are published online shortly after acceptance, before technical editing, formatting and proof reading. Using this free service, authors can make their results available to the community, in citable form, before we publish the edited article. This *Accepted Manuscript* will be replaced by the edited, formatted and paginated article as soon as this is available.

You can find more information about *Accepted Manuscripts* in the [Information for Authors](#).

Please note that technical editing may introduce minor changes to the text and/or graphics, which may alter content. The journal's standard [Terms & Conditions](#) and the [Ethical guidelines](#) still apply. In no event shall the Royal Society of Chemistry be held responsible for any errors or omissions in this *Accepted Manuscript* or any consequences arising from the use of any information it contains.

Fabrication of coral like carbon black/MnO₂ nano composites from commercial carbon black and its application in supercapacitors

Junwei An^a, Xiaoqiang Peng^b, Shengming Xu^{a, c*}, Zhenghe Xu^{a, d*}, Jianlong Wang^{a, c}

^aInstitute of Nuclear and New Energy Technology, Tsinghua University, Beijing, China

^bKunming University of Science and Technology, Kunming, China

^cBeijing Key Lab of Fine Ceramics, Tsinghua University, China

^dDepartment of Chemical and Materials Engineering, University of Alberta, Edmonton, AB,
Canada

*TO whom should be corresponded to: smxu@tsinghua.edu.cn (S. Xu) ; zhenghe@ualberta.ca (Z.
Xu)

Abstract:

A carbon black/MnO₂ nano-composite (CB/MnO₂) of coral-like architecture was synthesized from a commercially available conductive carbon black (CB) using an in-situ method. The morphology and structure analysis of the synthesized CB/MnO₂ revealed 10 nm thick MnO₂ nano-sheets grown on the CB. The MnO₂ nano-sheets of poor-crystalline δ -MnO₂ birnessite structure assembled into a coral-like architecture. Energy dispersive X-ray (EDX) microanalysis showed high Mn content in the composite. The electrochemical tests using the synthesized the CB/MnO₂ showed a specific capacitance of 946F/g at a current density of 0.3A/g, which was much higher than that of the composites reported in the literature. Under a current density of 30A/g, the CB/MnO₂ electrode was shown to retain a high specific capacitance after 5000 charge/ discharge cycles. The results from this study demonstrate that the CB/MnO₂

nano composite materials of coral-like architecture fabricated with commercially available CB and MnO₂ achieved a good electrochemical performance, exhibiting promising application prospects.

1 Introduction:

The rapid depletion of non-renewable fossil energy sources along with severe pollution and greenhouse emission due to their industrial utilization have caused an exponential increase in searching for renewable and clean energy sources, such as solar, wind, hydro, etc.¹⁻³ In order to make full use of the power produced by renewable energy, it is necessary to develop advanced energy storage technologies⁴. Supercapacitors and lithium-ion batteries are known new energy storage devices that are currently being researched widely to improve their performance and affordability⁵⁻¹⁰. Lithium-ion batteries have a distinct advantage in terms of energy density, which is favorable for electric vehicles, hybrid cars, etc.^{11,12} However, the current lithium-ion batteries suffer from not only a low power discharge density and slow charging speed, but also poor safety performance, which severely limits their use^{13,14}. In contrast, electric double layer (EDL) supercapacitors feature a good discharge power density and great safety performance,^{1,15} but suffer from low energy density^{2,16}. In order to increase the energy density of EDL supercapacitors, an asymmetric electrode supercapacitor has to be made to achieve a stable cycling performance¹⁷⁻¹⁹. Another approach is to fabricate symmetric electrode supercapacitors by employing pseudo-supercapacitor materials with EDL supercapacitor materials, such as transition metal oxide hybrids with a carbon-based

material.²⁰⁻²⁵ The large pseudo capacitance of the transition metal oxides and the high cycling properties of the carbon based materials is an advantage.^{15, 26-30}

There has been extensive research on carbon nanotubes (CNTs) and graphene, which demonstrated good performance, including infinite carrier concentration density, good electric conductivity, large specific surface area (SSA), good corrosion resistance and excellent mechanical properties^{14, 25, 28, 31-35}. To date, it has been reported extensively in the literature that graphene hybrid MnO₂ composite³⁶⁻³⁸ and CNT-fabricated MnO₂ composites^{19, 39, 40} have good energy capacity and high power density and long-term cycling stability.^{39, 41}

The good electrochemical performance of hybrid electrode materials fabricated with graphene or CNTs and MnO₂ has been attributed to the good conductivity of carbon-containing materials,⁴²⁻⁴⁵ huge SSA,⁴⁶ great chemical durability and the special structure constructed by the graphene or CNT with MnO₂ on a nanometer scale,^{34, 47} which presents an intimate contact between the carbon material with the transition metal oxide.^{24, 47} This special structure efficiently accumulates and utilizes the charges created by the surficial pseudo-capacitance reaction of the MnO₂.⁴⁸ It should be noted that both the graphene and the CNTs are very expensive,⁴⁹ and they often contain impurities from their production processes which generate chemical waste.⁵⁰ The Hummers method employed to produce graphene uses a large amount of sulfuric acid, hydrochloric acid, potassium permanganate, etc.⁵¹ All these substances need to be removed from the graphene oxide solution, which inevitably generates hazardous waste to the environment.

Commercially available high conductivity carbon black (CB), commonly used as a conductive agent when assembling lithium ion battery or supercapacitors,⁵²⁻⁵⁴ is cheap (about \$15 per kilogram of coconut shell and activated carbon supercapacitor that the manufacturers use)⁵⁵ and readily available.^{49, 56} In addition to chemical durability, the conductivity and SSA of CB is around 6000 S/m and 1200 m²/g, respectively, it is common and comparable with that of the reduced graphene oxide or CNTs, if not better. In this paper, we propose the use of high conductivity CB as a base material to grow MnO₂ with a coral-like morphology. In this structure, the CB acts as an EDL material, while the MnO₂ nano-layer grown on the CB functions as a pseudo-capacitive material in the formed coral globular structure and is intimately combined as a CB/MnO₂ composite material. The coral structure creates a large SSA and possibly a high specific capacitance due to the occurrence of adequate pseudo-capacitive reaction of MnO₂.⁵⁷ The high conductivity and huge SSA of the CB provide an unobstructed charge transport channel.⁵⁸ The efficient collection of charge through these transport channels results in a high specific capacitance or energy density, while preventing the structure collapse caused by charge accumulation. These distinct features are desirable for the high cycle stability of the coral like CB /MnO₂ battery materials.⁵⁸⁻⁶⁰

2. Experimental Section

2.1 Preparation of the coral like CB/MnO₂ nano-sheet composites:

The method to prepare the MnO₂ nano-layer was based on previous research.⁶¹ In this in-situ method, commercial CB was used as a scaffold on which a MnO₂

nano-layer grew, producing a coral spherical CB/MnO₂ nano-sheet composite material. Under moderate stirring, 0.1 g of CB was added to 100 ml of a 1M KMnO₄ aqueous solution, followed by a drop wise addition of a 2 ml solution of 0.05M sodium dodecyl benzene sulfonate (SDBS). The mixture was stirred for 15 min and then sonicated in an ultrasonic bath for 30 min. The resulting solution was stirred at high speed for 3 min before being transferred into a 150ml autoclave and heated at 160°C for 5 h. The final product was filtrated and washed with 200 ml of ethanol and 500 ml of deionized water. After drying at 80 °C for 24 h and pulverizing, the round coral CB/MnO₂ nano-sheet composite powder was obtained.

2.2 Material characterization.

Transmission electron microscopy (TEM), scanning electron microscopy (SEM) and X-ray diffraction (XRD) were used to characterize the texture, morphology and chemical structure of the CB and CB/MnO₂ nano-sheet composite. TEM measurements were carried out on a JEOL 200 TEM at 100 kV and a Tecnai G2 F20 S-TWIN TEM at 200 kV. TEM samples were prepared by dropping a small volume of a diluted suspension on a 300 mesh copper grid covered with a thin amorphous carbon film. SEM measurements were carried out on a HITACHI S-4800 SEM. The SEM samples were prepared by dropping ethanol-dispersed samples onto a conductive Si plate, followed by the evaporation of the solvent at room temperature. The XRD patterns of CB, MnO₂ and the CB/MnO₂ nano-sheet composites were recorded on a Rigaku Dmax 2400 X-ray diffractometer. The X-ray photoelectron spectroscopy (XPS) technique (Thermo escalab 250Xi) was employed to measure the chemical state and

electronic state of element Mn in CB/MnO₂ nano-sheet composite.

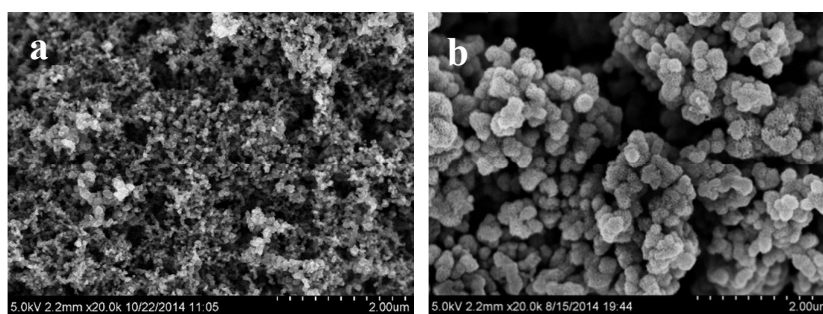
2.3 Measurement of the electrochemical properties:

As indicated in the literature,^{1, 58} the electrochemical measurements were conducted in a three-electrode system, using platinum sheet as counter electrode, an AgCl/Ag electrode as the reference electrode and a glassy-carbon electrode as the working electrode coated with samples which were impregnated with a 5% nafion solution. The working electrode was prepared by casting a nafion-impregnated sample onto a glassy-carbon electrode of 5 mm in diameter. Typically, a 20 mg sample was dispersed in 20 ml of ethanol solution containing 30 μ l 5 wt.% nafion in water under ultra-sonication for 15 minutes. A certain amount of sample solution was then placed onto the glassy-carbon electrode and dried at room temperature before the electrochemical test. The CB/MnO₂ nano composite material on the glassy-carbon electrode was about 10 microgram. The three-electrode system was used to evaluate the electrochemical performance by cyclic voltammetry (CV) and galvanostatic charge-discharge measurements on a CHI 660A potentiostation at 25 °C. The electrolyte was a 2 M Na₂SO₄ aqueous solution with pH=10.

3 Results and Discussion

Employing SEM and TEM, the morphology and texture of CB and CB/MnO₂ nano composite material were determined. The morphology of CB and CB/MnO₂ is shown in Figure 1. Figure 1a shows the spherical shape and smooth surface of the CB with an average diameter of about 30nm. Figure 1b shows the CB/MnO₂ morphology at the same scale as in Figure 1a where a uniform coral like MnO₂ nano-layers on the

surface of the CB can be observed. It can be seen that the MnO_2 grew on the surface of the CB and the size of the CB/MnO_2 was much larger than that of the original CB particles. Figure 1c and Figure 1d show the morphology of CB/MnO_2 nano composite particles before and after a long-term charge-discharge test at 30 A/g, respectively. Figure 1c shows a thickness of the MnO_2 nano-layer around 10 nm, featuring a coral-like architecture and an infrangible structure integrated with CB. The coral-like configuration of CB/MnO_2 , presents a multiple-void structure which can accommodate multiple electrolytes and facilitate the adequate pseudo-capacitive reaction from MnO_2 , and consequently enhancing the electrochemical performance.^{62,}
⁶³ Comparing Figure 1c with Figure 1d, it can be observed that after a long-term high current density charge-discharge process the structure of the CB/MnO_2 nano composite material does not change significantly. This observation demonstrates that the coral architecture of the CB/MnO_2 with MnO_2 grown on conductive CB has a good electrochemical stability, which was proven by the results of the following electrochemical tests.



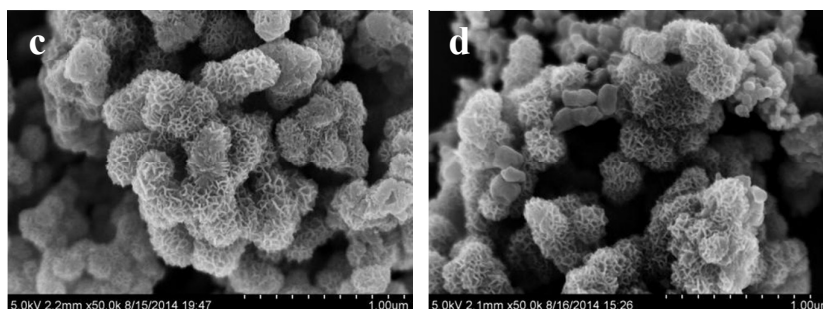


Fig. 1 SEM images of CB/MnO₂ and CB. a and b correspond to the images of CB and CB/MnO₂ composite at the same magnification, respectively. c and d show SEM images of CB/MnO₂ composite electrode before and after long-term charge-discharge tests.

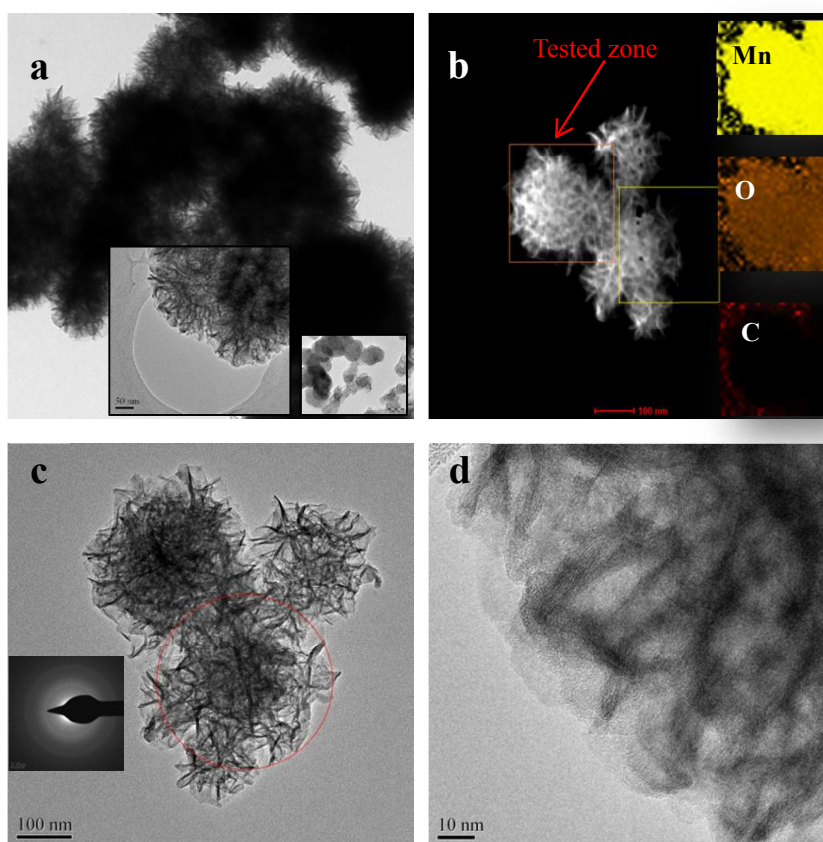


Fig.2 TEM images of CB/MnO₂. a shows the general image of CB/MnO₂, the small map insets in image a are CB (left) and CB/MnO₂ (right) with a scale bar of 50 nm. b shows the EDS spectrum of CB/MnO₂, the diagrams are the element content maps of Mn, O and C from the top to the bottom. c and d are the HRTEM images of the CB/MnO₂ nano composite particles.

Figure 2 shows the TEM images and energy dispersive X-ray spectra (EDX) of the CB/MnO₂ nano composite particles as prepared. Two small maps of the same scale in the inset of Figure 2a correspond to CB (left) and the CB/MnO₂ nano composite particles (right). The EDS scanning map of the CB/MnO₂ nano composite

particles is shown in Figure 2b, where the yellow diagram represents the map of Mn; the brown the map of O; and the red one, the map of C. The mass percentage of MnO₂ in the CB/MnO₂ composite was 89.40 wt%, which can be seen in the EDX test result. In the CB/MnO₂ nano composite particles, the C content was the lowest, while the Mn content was the highest. Figure 2c shows poor crystallinity or the amorphous nature of MnO₂ in the CB/MnO₂ nano composite particles. The image of electron diffraction lattice stripe measurement in Figure 2d also shows the relatively weak crystallinity of the CB/MnO₂ nano composite particles. The poor crystallinity of MnO₂ may be attributed to the extremely thin nature of nano MnO₂ sheets in the CB/MnO₂ nano composite particles. The thickness of the MnO₂ sheet on the CB/MnO₂ nano composite particles was estimated to be only around 10 nm. The thin nature of these nano-sheets limits the repeating arrangement of the MnO₂ lattice, a great limitation of the current preparation method of the CB/MnO₂ nano composite particles. Despite the poor crystallinity, the lattice spacing of the nano MnO₂ sheet was estimated from the image in Figure 2d to be 0.275nm.

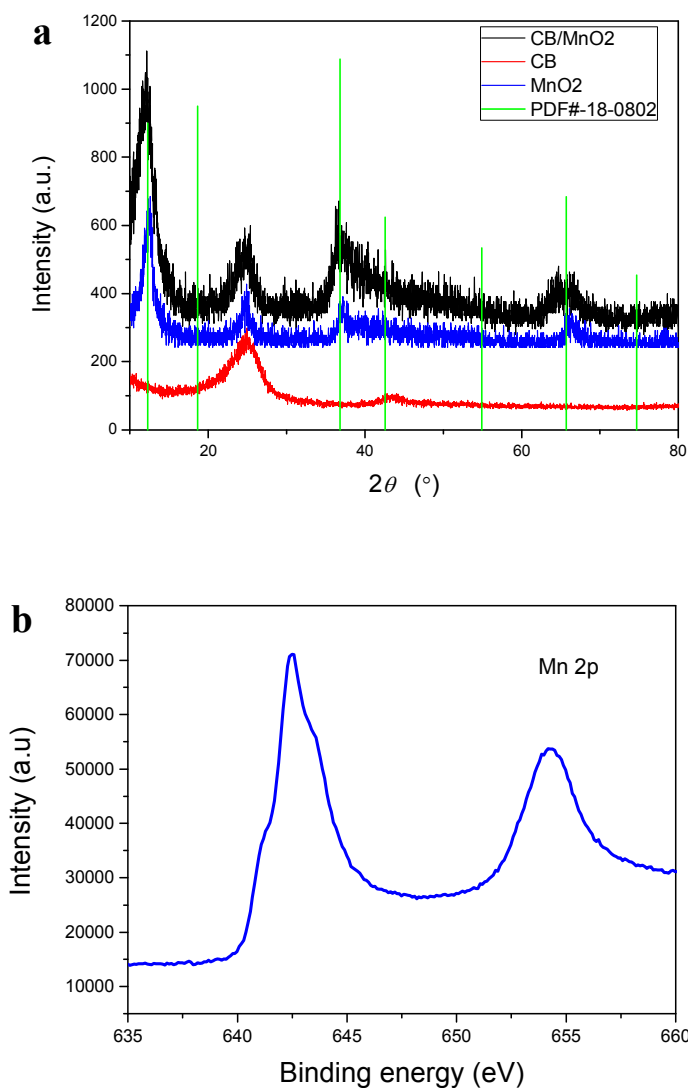


Fig.3 a, XRD patterns of CB/MnO₂, CB and MnO₂. b, XPS spectrum of Mn in CB/MnO₂

The crystal structures of the CB/MnO₂, the pure MnO₂ and CB were analyzed by XRD. The XRD patterns of the CB/MnO₂, MnO₂ and CB are shown in Figure 3a. The 2θ diffraction peaks of CB/MnO₂ are located at 12.282°, 36.803° and 65.700°. The diffraction peaks for bulk MnO₂ and MnO₂ nano-sheet on CB correspond well to the standard diffraction peaks given in a standard JCPDS card (No. 18-0802) for δ -MnO₂.⁵⁷ Also shown in Figure 3 are broader diffraction peaks for MnO₂ and CB/MnO₂, most likely as a result of the poor polycrystalline or amorphous nature of the nano MnO₂

sheet on the CB/MnO₂ nano composite particles. The structure of CB was also characterized by XRD. The result showed a major diffraction peak of CB at 26.2°, corresponding to the characteristic peak of the hexagonal carbon in a standard JCPDS card (No.75-1621). In Figure 3b, the result of XPS test reveals the valance state of Mn is 4⁺ (as MnO₂) in CB, which can be seen in reference⁶⁴.

The electrochemical characteristics of CB, CB/MnO₂ and MnO₂ were determined using cyclic voltammetry (CV), Gavanostatic charge-discharge test and AC impedance (EIS) measurement. Figure 4 shows the CV curves for CB/MnO₂ and MnO₂ at the scanning rates of 2mV/s~ 50mV/s. Figure 4a shows rectangular CV curves for the CB/MnO₂ nano composite particles as prepared, illustrating a good capacitive performance under a low scanning rate (2mV/s). The absence of the redox peaks in the CV curves implies a good electrochemical reversibility. The shape of the CV curves changed significantly when the scanning rates increased from 2mV/s to 50mV/s. The current shift rates upon shift (decrease) of the scanning potential became smaller when the scan rate increased, which indicates a capacitive decay under high scanning rates.⁶³ For comparison, the measurement of the CV curves for the electrode made of MnO₂ powder only was attempted. Unfortunately, a poor electrical conductivity was obtained, which makes reading of the electrochemical test data impossible.⁶⁵ Therefore, the CV measurement was conducted using electrodes made of MnO₂ mixed with the conductive CB, with a certain amount of conductive CB being added in during the MnO₂ electrode preparation procedure. In the initial tests, the conductive CB nanoparticles were observed to accumulate on the outer surface of

the MnO₂. The results in Figure 4b obtained when the scan rate increased from 2mV/s to 50mV/s show a pair of obvious redox peaks, as well as a larger rectangular area as compared to the CV curves of CB/MnO₂ nano composite particles.²⁶ Upon the shift of the scanning potential, the current shift rate did not decrease significantly, indicating a better ability of charge storage.⁶⁶ The rectangle area for the MnO₂ electrode was larger than that obtained with the electrode made of the CB/MnO₂ nano composite particles.⁶⁷ This was due to the poorly conductive MnO₂ layer that lay outside of the CB/MnO₂ nano composite material, while the highly conductive CB lay in the core. When the scanning rate increased, the CB/MnO₂ cannot fully display its electrochemical reversibility and good capability of current steering rate. On the contrary, following a traditional way of making electrodes, conductive CB was added in by physically mixture. In this way, in the MnO₂ electrode, the conductive CB particles accumulate outside the MnO₂ nano-lamella, as mentioned before. Through the contact of conductive CB particles and formation of conductive network, the MnO₂ electrode shows a pair of obvious redox peaks and illustrates a larger current steering rate, in addition to a larger rectangle area than that of the CB/MnO₂.

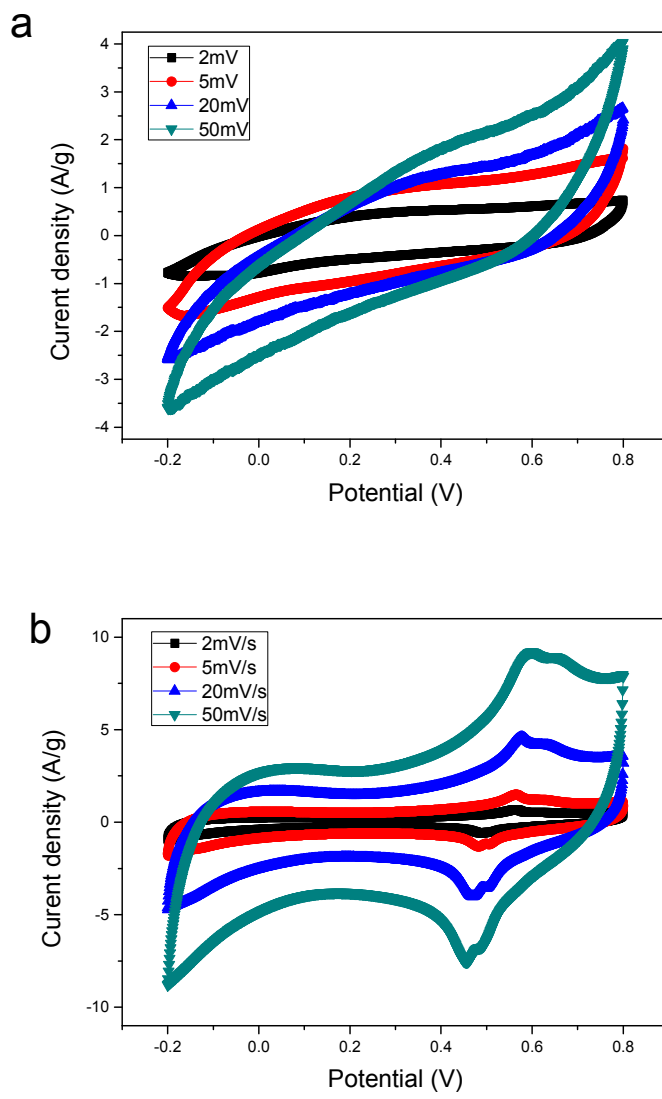


Fig. 4 CV curves of CB/MnO₂ and MnO₂ at different scanning rates: a for the CB/MnO₂ nano composite particles, and b for the bulk MnO₂.

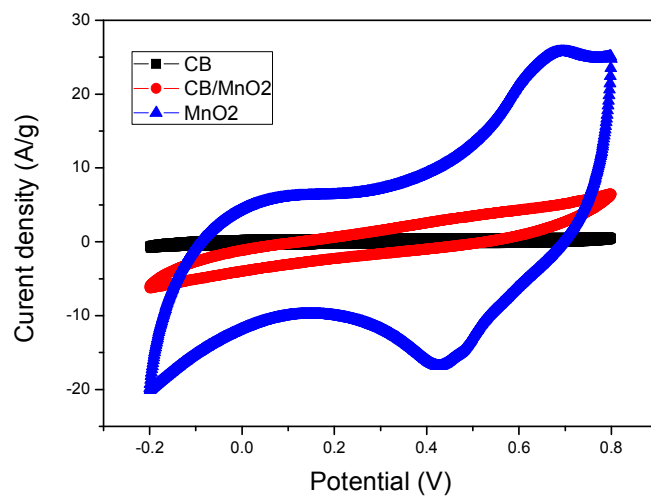


Fig. 5 CV curves of CB, origin MnO₂ and CB/MnO₂ nano composite particle at scanning rate of 200mV/s

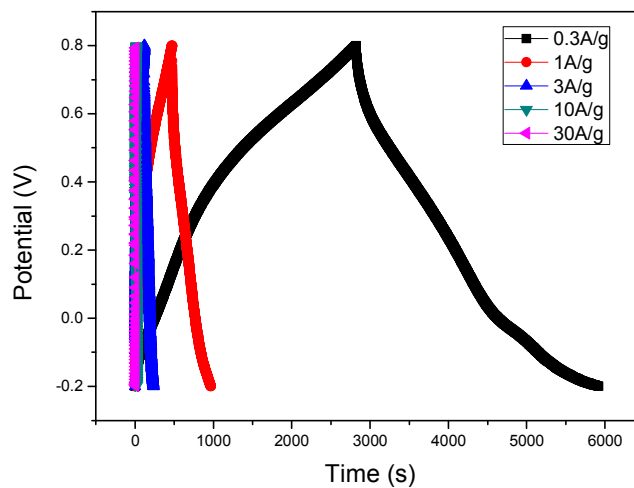


Fig. 6 Charge-discharge curves of CB/MnO₂ nano composite particles at different current densities

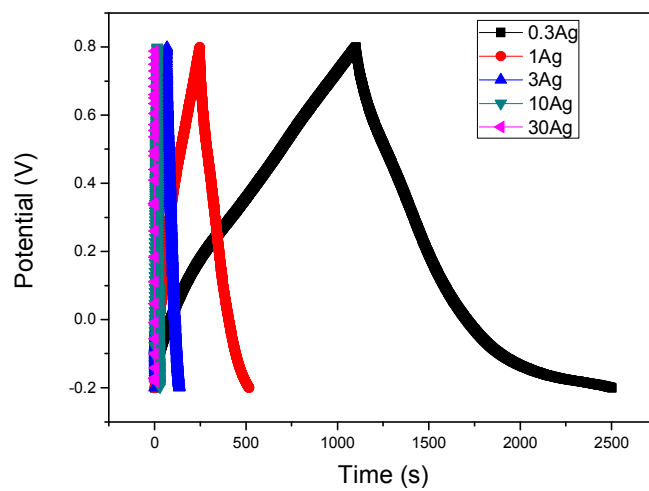


Fig. 7 Charge-discharge curves of MnO₂ at different current densities

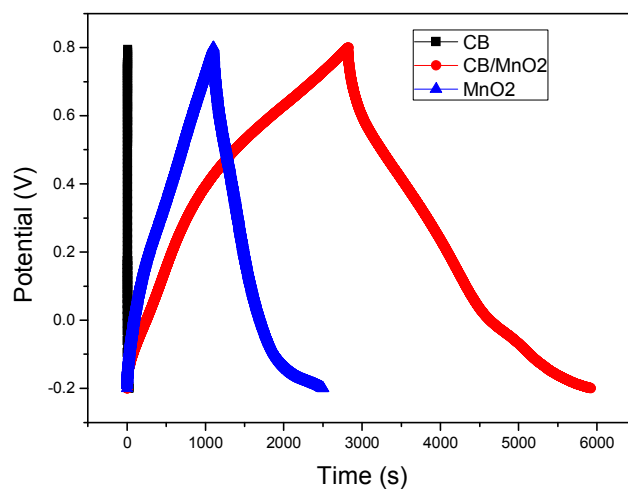


Fig. 8 Charge-discharge curves of CB, MnO₂ and CB/MnO₂ nano composite particles at current density of 0.3A/g

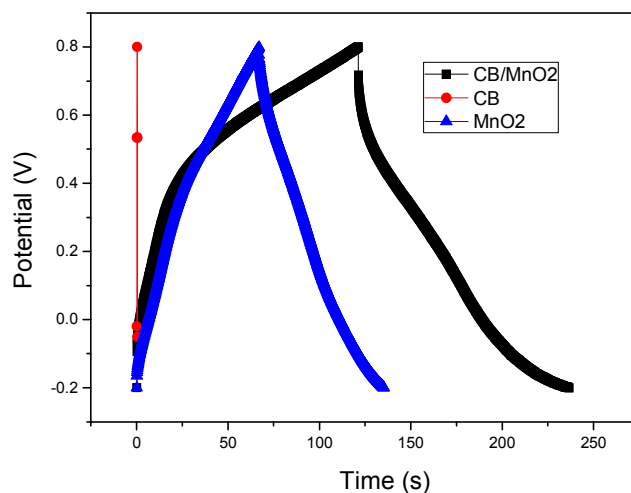


Fig. 9 Charge-discharge curves of CB, MnO₂ and CB/MnO₂ nano composite particles at current density of 3A/g

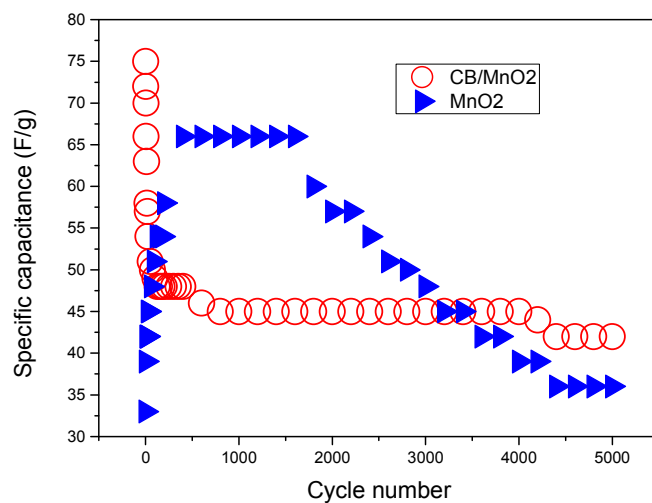


Fig. 10 Long-term charge-discharge cycling test plots of coral shape CB/MnO₂ nano composite and pure MnO₂

In order to study the electrochemical behavior of the CB/MnO₂ nano composite particles and MnO₂ (it has been mixed with CB to improve its conductivity when test its electrochemical performances) electrodes more clearly, CV curves of CB/MnO₂ nano composite particles and MnO₂ at scanning rate of 200mV/s were compared. As seen in Figure 5, a pair of distinct redox peaks present in CV curve of CB/MnO₂ nano

composite particle suggests a redox reaction conversion process. However, when compared with the CV curve of the MnO₂ electrode with CB particles directly mixed in, it was found that the rectangular area was larger than that of the CB/MnO₂ nano composite particle electrode. The CV curve of the MnO₂ electrode presents two obvious redox peaks, corresponding to the redox reaction of MnO₂. At the same time, its rectangle area was much larger than that of the CB/MnO₂ nano composite particle and pure CB, which suggests that the conductive CB physically mixed with MnO₂ and could have a higher capacitance. It should be noted that, for the MnO₂ electrode, due to the accumulation of conductive CB on the MnO₂ nano-layer surface, the mutual inter-atomic force was far less than that of the interior binding force between CB and MnO₂ in the CB/MnO₂ nano composite particle prepared by the in-situ growth method. Therefore, the MnO₂ electrode physically mixed with conductive CB accumulating on its surface should possess a structure instability problem, which may lead to large capacity attenuation in the long-term charge-discharge process.

Figure 6 and 7 exhibit the Galvano-static charge and discharge curves of pure CB and the CB/MnO₂ nano composite particle under different current densities. After calculations following a formula referred in the literature⁶⁸, it was found that the specific capacitance of the CB/MnO₂ nano composite particle was 946F/g at a current density of 0.3A/g, much higher than that of the MnO₂ electrode (420F/g). It illustrates that the CB/MnO₂ nano composite particle grown by an in-situ growth route could achieve a much higher capacitance under high current density than that of the MnO₂ electrode with conductive CB directly mixed in. After calculations, it was found that

the specific capacity of the CB/MnO₂ nano composite particle was 500 F/g at a current density of 1A/g and 354F/g at 3A/g as well as 90F/g at a much higher current density of 30A/g. The specific capacity of the MnO₂ electrode with CB accumulating on its surface was 270F/g (1A/g), 112F/g at 3A/g and 42F/g at 30A/g. It can be seen that, under high current density, the CB/MnO₂ nano composite particle electrode demonstrates a higher capacitance performance than that of the MnO₂ electrode, which can be attributed to the excellent coral structure of the CB/MnO₂ nano composite particle.

To study the electrochemical properties of pure CB, the MnO₂ electrode and the CB/MnO₂ nano composite particle, their Gavanostatic charge-discharge curves at current densities of 0.3A/g and 3A/g are shown in Figure 8 and Figure 9, respectively. It can be noted that at different current densities, the specific capacitance of both the pure CB and the MnO₂ electrode were much lower than that of the CB/MnO₂ nano composite particle. Especially, in Figure 8 and Figure 9, the CB/MnO₂ nano composite particle exhibits much longer discharge time than that of the MnO₂ electrode which demonstrates that the CB/MnO₂ nano composite particle of coral structure could efficiently utilize the highly conductive CB by effectively transferring faraday charge from the surface of the coral MnO₂ nano-layer to the collector, which consequently performs at a high capacitance.^{69, 70} Additionally, compared to the reported data the as prepared CB/MnO₂ nano composite particle (946F/g) performs at a higher specific capacity at the current density of 0.3A/g than that of the graphene/MnO₂ composites,^{71, 72} and that of the CNT/MnO₂ composites^{73, 74}.

As seen from Figure 8 and Figure 9, at current densities of 0.3 A/g and 3 A/g, the galvanostatic charge-discharge curves of the CB/MnO₂ illustrate a symmetrical triangle shape, which indicates a good charge and discharge reversible capacity.^{58, 63} These results correspond to the CV curves at different scanning rates which are shown in Figure 4. These phenomenon in charge-discharge tests and CV tests of the CB/MnO₂ nano composite material suggest that the CB/MnO₂ has good electrochemical cycling stability.⁵⁸

The electrochemical stability of the CB/MnO₂ nano composite material was investigated by a long-term charge-discharge cycling test at a high current density of 30A/g. After cycling 5000 times, the CB/MnO₂ still retained 56% of its initial capacity, which is shown in Figure 10. This suggests that the CB/MnO₂ nano composite material possesses a higher reserved specific capacitance than that of MnO₂ and has good electrochemical cycle stability. The morphology comparison of the CB/MnO₂ nano composite material before and after 5000 times charge-discharge process demonstrated its good electrochemical cycle stability (shown in Figure 1c and 1d). As shown in Figure 1c and 1d, it can be observed that after long-term charge-discharge cycles, most of the CB/MnO₂ nano composite material was covered by MnO₂ nano-layers, only some MnO₂ nano-layers collapsed and a few spherical CB particles were exposed. This verified that the CB/MnO₂ nano composite material with coral structure can comprehensively utilize the high conductivity of CB and the high capacitance of the MnO₂ nano-layer, which synergistically enhance its specific capacitance and stable electrochemical cycling performance. In Figure 10, it is

notable that the MnO_2 electrode showed an intensified specific capacitance in the early stage of the long-term charge-discharge process. However, when the charge-discharge process continued, its capacitance decreased rapidly, as found in the literature.⁶⁵ Compared to MnO_2 electrode, the CB/MnO_2 composite showed a better electrochemical cycling stability, which can be attributed to the special architecture of the CB/MnO_2 composite, in which the CB acts as a high conductivity nucleus and the MnO_2 nano-layer acts as a faradic reaction shell.

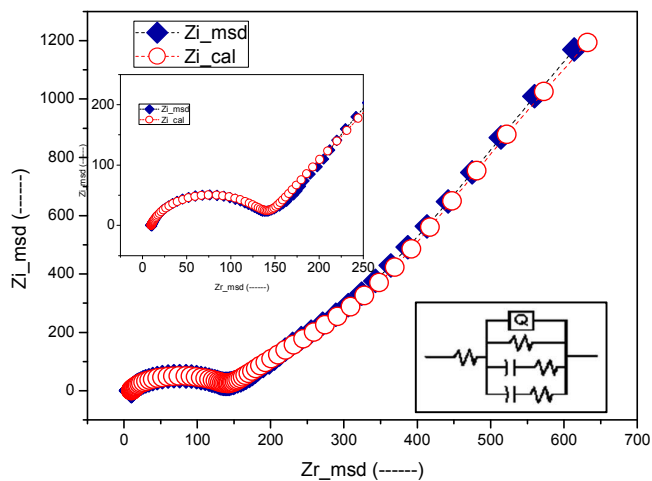


Fig. 11 EIS curves of CB/MnO_2 nano composite material before long-term high current density charge-discharge test process

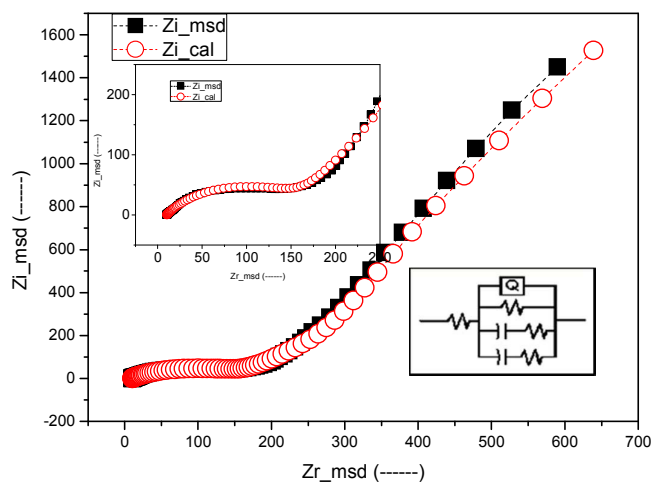


Fig. 12 EIS curves of coral shape CB/MnO₂ nano composite material after long-term high current density charge-discharge test process

Using EIS technology, the impedance spectra of the CB/MnO₂ nano composite material before and after long-term charge-discharge cycling process at a high current density of 30A/g was obtained and shown in Figure 11 and Figure 12, respectively. The red hollow curve shows the analog curve and the insets semicircle shows the high frequency area of the EIS spectrum, as well as the analog circuit diagram inset the spectrum below. From Figure 11, it is known that the CB/MnO₂ nano composite material had an electrolyte resistance (R_e) of 7.5 Ω and a charge transfer resistance (R_{ct}) of 132 Ω . After a 5000 cycling charge-discharge process, its R_e was still 7.5 Ω , but R_{ct} increased to 152 Ω . The electrolyte resistance of CB/MnO₂ exhibited no obvious change, and its charge transfer resistance R_{ct} varied very little. This suggests that the charge transfer path of the CB/MnO₂ nano composite material had little obstruction after a long-term charge-discharge process at a high current density.^{1,75} However, it should be noted that the slope of its Warburg curve changed a lot after the long-term charge and discharge cycles at high current density. This suggests that the electrolyte

ion diffusion became difficult in the electrode surface caused by Warburg impedance, illustrating an increase in the capacitance resistance and electrical resistance of the CB/MnO₂ after a long-term charge and discharge process.

Conclusion:

Using the in-situ growth method, a coral architecture CB/MnO₂ nano composite material was prepared. According to SEM and TEM results, it was found that the morphology of CB/MnO₂ only had some collapse after a long-term charge-discharge cycle. EDX results confirm that the carbon content in the composite material was low, manganese was the highest in content and there was a moderate amount of oxygen content. Electron diffraction analysis shows that the MnO₂ in CB/MnO₂ presents poor crystallinity, due to its nano-lamellar structure and XRD tests prove the birnessite structure of δ - MnO₂ in CB/MnO₂. The rectangular area of the CB/MnO₂ CV curve was smaller than that of the MnO₂ directly mixed with conductive CB. However, at a current density of 0.3A/g, the specific capacitance of CB/MnO₂ was 946F/g, higher than that of MnO₂ (420F/g). This demonstrates that the CB/MnO₂ where the MnO₂ was grown in-situ on CB had a high capacitance at high current density. After 5000 cycles of charge-discharge process at a current density of 30A/g, it can be observed that CB/MnO₂ had a retention capacitance of 42F/g, keeping 56% of its initial capacitance, demonstrating good electrochemical cycle stability.

Acknowledgements

This work was supported by the National Nature Science Foundation of China (51274130, S. Xu), the Recruitment Program of Global Experts (Z. Xu), and the

Program for Changjiang Scholars and Innovative Research Team in University
(IRT13026, J. Wang)

References

1. K. Zhang, L. L. Zhang, X. S. Zhao and J. S. Wu, *Chem Mater*, 2010, **22**, 1392-1401.
2. J. Yan, T. Wei, B. Shao, Z. J. Fan, W. Z. Qian, M. L. Zhang and F. Wei, *Carbon*, 2010, **48**, 487-493.
3. X. Chen, N. Q. Zhang and K. N. Sun, *Prog Chem*, 2011, **23**, 2045-2054.
4. F. Han, A. H. Lu and W. C. Li, *Prog Chem*, 2012, **24**, 2443-2456.
5. M. H. Chakrabarti, C. T. J. Low, N. P. Brandon, V. Yufit, M. A. Hashim, M. F. Irfan, J. Akhtar, E. Ruiz-Trejo and M. A. Hussain, *Electrochim Acta*, 2013, **107**, 425-440.
6. Y. Gao, Y. S. Zhou, M. Qian, H. M. Li, J. Redepenning, L. S. Fan, X. N. He, W. Xiong, X. Huang, M. Majhouri-Samani, L. Jiang and Y. F. Lu, *Rsc Adv*, 2013, **3**, 20613-20618.
7. G. Q. Han, Y. Liu, E. J. Kan, J. Tang, L. L. Zhang, H. H. Wang and W. H. Tang, *Rsc Adv*, 2014, **4**, 9898-9904.
8. N. Li, J. Y. Wang, Z. Q. Liu, Y. P. Guo, D. Y. Wang, Y. Z. Su and S. Chen, *Rsc Adv*, 2014, **4**, 17274-17281.
9. X. Y. Li, Y. M. Chen, H. M. Yao, X. Y. Zhou, J. Yang, H. T. Huang, Y. W. Mai and L. M. Zhou, *Rsc Adv*, 2014, **4**, 39906-39911.
10. Y. R. Kang, F. Cai, H. Y. Chen, M. H. Chen, R. Zhang and Q. W. Li, *Prog Chem*, 2014, **26**, 1562-1569.
11. J. F. Ni, H. H. Zhou, J. T. Chen and G. Y. Su, *Prog Chem*, 2004, **16**, 335-342.
12. Y. F. Deng, L. N. Wan, Y. Xie, X. S. Qin and G. H. Chen, *Rsc Adv*, 2014, **4**, 23914-23935.
13. Z. X. Chen, M. Zhou, Y. L. Cao, X. P. Ai, H. X. Yang and J. Liu, *Adv Energy Mater*, 2012, **2**, 95-102.
14. K. T. Lee, S. Jeong and J. Cho, *Accounts Chem Res*, 2013, **46**, 1161-1170.
15. X. X. Sun, H. J. Wang, Z. B. Lei, Z. H. Liu and L. L. Wei, *Rsc Adv*, 2014, **4**, 30233-30240.
16. H. J. Liu and Y. Y. Xia, *Prog Chem*, 2011, **23**, 595-604.
17. T. Brousse, P. L. Taberna, O. Crosnier, R. Dugas, P. Guillemet, Y. Scudeller, Y. Zhou, F. Favier, D. Belanger and P. Simon, *J Power Sources*, 2007, **173**, 633-641.
18. J. Chang, M. Jin, F. Yao, T. H. Kim, V. T. Le, H. Yue, F. Gunes, B. Li, A. Ghosh, S. Xie and Y. H. Lee, *Adv Funct Mater*, 2013, **23**, 5074-5083.
19. Z. Y. Zhang, F. Xiao, L. H. Qian, J. W. Xiao, S. Wang and Y. Q. Liu, *Adv Energy Mater*, 2014, **4**.
20. K. Naoi, *Fuel Cells*, 2010, **10**, 825-833.
21. W. J. Huang, T. Y. Yao, Q. L. Hao, W. J. Wang, X. F. Xia and X. Wang, *Rsc Adv*, 2014, **4**, 56615-56624.
22. Y. Su and I. Zhitomirsky, *J Power Sources*, 2014, **267**, 235-242.
23. D. P. Dubal, P. Gomez-Romero, B. R. Sankapal and R. Holze, *Nano Energy*, 2015, **11**, 377-399.
24. P. Simon and Y. Gogotsi, *Nat Mater*, 2008, **7**, 845-854.

25. Y. P. Zhai, Y. Q. Dou, D. Y. Zhao, P. F. Fulvio, R. T. Mayes and S. Dai, *Adv Mater*, 2011, **23**, 4828-4850.
26. J. H. Liu, J. W. An, Y. C. Zhou, Y. X. Ma, M. L. Li, M. Yu and S. M. Li, *Acs Appl Mater Inter*, 2012, **4**, 2870-2876.
27. J. Tang, H. M. Meng and L. L. Huang, *Rsc Adv*, 2014, **4**, 16512-16516.
28. H. Jiang, P. S. Lee and C. Z. Li, *Energ Environ Sci*, 2013, **6**, 41-53.
29. S. He and W. Chen, *Journal of Power Sources*, 2015, **294**, 150-158.
30. S. He and W. Chen, *Journal of Power Sources*, 2014, **262**, 391-400.
31. A. K. Geim and K. S. Novoselov, *Nat Mater*, 2007, **6**, 183-191.
32. M. Koch, F. Ample, C. Joachim and L. Grill, *Nature Nanotechnology*, 2012, **7**, 713-717.
33. A. Javey, J. Guo, Q. Wang, M. Lundstrom and H. J. Dai, *Nature*, 2003, **424**, 654-657.
34. F. Beguin, V. Presser, A. Balducci and E. Frackowiak, *Adv Mater*, 2014, **26**, 2219-2251.
35. B. C. Wood, T. Ogitsu, M. Otani and J. Biener, *Journal of Physical Chemistry C*, 2014, **118**, 4-15.
36. N. Kurra, S. Kiruthika and G. U. Kulkarni, *Rsc Adv*, 2014, **4**, 20281-20289.
37. X. C. Dong, X. W. Wang, L. Wang, H. Song, X. G. Li, L. H. Wang, M. B. Chan-Park, C. M. Li and P. Chen, *Carbon*, 2012, **50**, 4865-4870.
38. S. He and W. Chen, *Nanoscale*, 2015, **7**, 6957-6990.
39. J. H. Zhang, Y. H. Wang, J. B. Zang, G. X. Xin, Y. G. Yuan and X. H. Qu, *Carbon*, 2012, **50**, 5196-5202.
40. L. B. Hu, W. Chen, X. Xie, N. A. Liu, Y. Yang, H. Wu, Y. Yao, M. Pasta, H. N. Alshareef and Y. Cui, *Acs Nano*, 2011, **5**, 8904-8913.
41. S. Hassan, M. Suzuki, S. Mori and A. Abd El-Moneim, *J Power Sources*, 2014, **249**, 21-27.
42. Y. He, W. Chen, X. Li, Z. Zhang, J. Fu, C. Zhao and E. Xie, *ACS Nano*, 2012, **7**, 174-182.
43. C. Choi, S. H. Kim, H. J. Sim, J. A. Lee, A. Y. Choi, Y. T. Kim, X. Lepro, G. M. Spinks, R. H. Baughman and S. J. Kim, *Sci Rep-Uk*, 2015, **5**.
44. W. X. Li, X. Y. Cui, R. Zeng, G. D. Du, Z. Q. Sun, R. K. Zheng, S. P. Ringer and S. X. Dou, *Sci Rep-Uk*, 2015, **5**.
45. T. Chen and L. Dai, *Mater Today*, 2013, **16**, 272-280.
46. J. Yan, Q. Wang, T. Wei and Z. J. Fan, *Adv Energy Mater*, 2014, **4**.
47. J. H. Chae, K. C. Ng and G. Z. Chen, *PI Mech Eng a-J Pow*, 2010, **224**, 479-503.
48. S. He, C. Hu, H. Hou and W. Chen, *Journal of Power Sources*, 2014, **246**, 754-761.
49. L. Weinstein and R. Dash, *Mater Today*, 2013, **16**, 356-357.
50. B. Xu, H. Zhang, G. P. Cao, W. F. Zhang and Y. S. Yang, *Prog Chem*, 2011, **23**, 605-611.
51. W. S. Hummers and R. E. Offeman, *Journal of the American Chemical Society*, 1958, **80**, 1339-1339.
52. Z. N. Yu, B. Duong, D. Abbitt and J. Thomas, *Adv Mater*, 2013, **25**, 3302-3306.
53. G. H. Yu, L. B. Hu, M. Vosgueritchian, H. L. Wang, X. Xie, J. R. McDonough, X. Cui, Y. Cui and Z. N. Bao, *Nano Lett*, 2011, **11**, 2905-2911.
54. J. Y. Luo and Y. Y. Xia, *Adv Funct Mater*, 2007, **17**, 3877-3884.
55. L. Weinstein and R. Dash, *Mater Today*, 2013, **16**, 356-357.
56. M. Vangari, T. Pryor and L. Jiang, *J Energ Eng*, 2013, **139**, 72-79.
57. S. Devaraj and N. Munichandraiah, *J Phys Chem C*, 2008, **112**, 4406-4417.
58. J. An, J. Liu, Y. Zhou, H. Zhao, Y. Ma, M. Li, M. Yu and S. Li, *The Journal of Physical*

- Chemistry C*, 2012, **116**, 19699-19708.
59. C. X. Guo and C. M. Li, *Energ Environ Sci*, 2011, **4**, 4504-4507.
 60. Z. B. Lei, N. Christov and X. S. Zhao, *Energ Environ Sci*, 2011, **4**, 1866-1873.
 61. J. Liu, J. Jiang, C. Cheng, H. Li, J. Zhang, H. Gong and H. J. Fan, *Adv Mater*, 2011, **23**, 2076-2081.
 62. J. An, J. Liu, Y. Ma, R. Li, M. Li, M. Yu and S. Li, *Eur Phys J-Appl Phys*, 2012, **58**.
 63. J. H. Liu, J. W. An, Y. X. Ma, M. L. Li and R. B. Ma, *J Electrochem Soc*, 2012, **159**, A828-A833.
 64. M. C. Biesinger, L. W. M. Lau, A. R. Gerson and R. S. C. Smart, *Applied Surface Science*, 2010, **257**, 887-898.
 65. T. M. Higgins, D. McAteer, J. C. M. Coelho, B. M. Sanchez, Z. Gholamvand, G. Moriarty, N. McEvoy, N. C. Berner, G. S. Duesberg, V. Nicolosi and J. N. Coleman, *ACS Nano*, 2014, **8**, 9567-9579.
 66. L. L. Zhang and X. S. Zhao, *Chem Soc Rev*, 2009, **38**, 2520-2531.
 67. Q. F. Zhang, E. Uchaker, S. L. Candelaria and G. Z. Cao, *Chem Soc Rev*, 2013, **42**, 3127-3171.
 68. X. Wang, Y. Zhang, C. Zhi, X. Wang, D. Tang, Y. Xu, Q. Weng, X. Jiang, M. Mitome, D. Golberg and Y. Bando, *Nat Commun*, 2013, **4**.
 69. Y. Huang, J. J. Liang and Y. S. Chen, *Small*, 2012, **8**, 1805-1834.
 70. D. P. Dubal, J. G. Kim, Y. Kim, R. Holze, C. D. Lokhande and W. B. Kim, *Energy Technol-Ger*, 2014, **2**, 325-341.
 71. B. G. Choi, Y. S. Huh, W. H. Hong, H. J. Kim and H. S. Park, *Nanoscale*, 2012, **4**, 5394-5400.
 72. G. H. Yu, L. B. Hu, N. A. Liu, H. L. Wang, M. Vosgueritchian, Y. Yang, Y. Cui and Z. A. Bao, *Nano Lett*, 2011, **11**, 4438-4442.
 73. J. Chen, C. Y. Jia and Z. Q. Wan, *Electrochim Acta*, 2014, **121**, 49-56.
 74. G. Y. Zhu, Z. He, J. Chen, J. Zhao, X. M. Feng, Y. W. Ma, Q. L. Fan, L. H. Wang and W. Huang, *Nanoscale*, 2014, **6**, 1079-1085.
 75. J. Jiang, Y. Y. Li, J. P. Liu, X. T. Huang, C. Z. Yuan and X. W. Lou, *Adv Mater*, 2012, **24**, 5166-5180.